Scilight

Hydrology and Water Resources
https://www.sciltp.com/journals/hwr

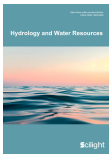

Supplementary Materials

Groundwater Storage as a Key Driver of Subannual Streamflow Variability

Yongqiang Zhang [1,*], Hongxing Zheng [2], Changming Liu [1], L. Ruby Leung [3], Chunmiao Zheng [4], Dongdong Kong [5] and Günter Blöschl [6]

[1] Key Laboratory of Water Cycle and Related Land Surface Processes, Institute of Geographic Sciences and Natural Resources Research, Chinese Academy of Sciences, Beijing 100101, China
[2] CSIRO Environment, Black Mountain, Canberra, ACT 2601, Australia
[3] Pacific Northwest National Laboratory, Richland, WA 99352, USA
[4] School of the Environment and Sustainable Engineering, Eastern Institute of Technology, Ningbo 315000, China
[5] Department of Atmospheric Science, School of Environmental Studies, China University of Geosciences, Wuhan 430074, China
[6] Institute of Hydraulic and Water Resources Engineering, Technische Universität Wien, Vienna 1040, Austria
* Correspondence: zhangyq@igsnrr.ac.cn

How To Cite: Zhang, Y.; Zheng, H.; Liu, C.; et al. Substantial Role of Groundwater Storage to Subannual Streamflow Variability. *Hydrology and Water Resources* **2025**, *1*(1), 2.

Performance of Multi-Temporal Framework

Figure S1 summarizes the performance of the multi-temporal attribution framework. The framework is shown to perform satisfactorily at all three temporal scales (monthly, seasonal and annual), as indicated by the fact that for 50%, 75% and 90% of catchments, the three drivers explain >68%, >53% and 37% of monthly, seasonal and annual streamflow variabilities, respectively. Comparison of model performance at the three temporal scales indicates that the framework works best at monthly scale, but similarly at seasonal and annual scales.

Figure S2 compares the annual streamflow variability estimated from the two climate drivers (precipitation, potential evaporation) and groundwater storage to the observed streamflow variability at the three temporal scales (monthly, seasonal, and annual). Overall, the estimated values correspond well to the observed values, with r^2 being 0.84, 0.60 and 0.88 at annual, seasonal and monthly scales, respectively.

Figures S3–S5 show more comprehensive results as they include the comparisons from three temporal scales (monthly, seasonal and annual) and three variables (P, S and PET) and the comparisons of relative contribution as well. Precipitation elasticity of streamflow increases from monthly to seasonal and to annual scale. On the contrary, catchment storage elasticity of streamflow decreases from monthly to seasonal and to annual scales. Potential evaporation elasticity of streamflow is more or less temporal-scale independent. Furthermore, the difference of precipitation elasticity of streamflow between monthly and seasonal scales is much smaller than that between monthly and annual scales and between seasonal and annual scales.

Similar to the precipitation elasticity of streamflow, the relative contribution of precipitation is much stronger at annual scale (or seasonal scale) than that at monthly scale. In contrast, the relative contribution of catchment storage is much stronger at monthly scale (or seasonal scale) than that at annual scale. The relative contribution of potential evaporation is similar at the three temporal scales. Overall, the relative difference at annual and monthly scale for potential evaporation is smaller than that for precipitation and catchment storage.

Figure S6 further compares the relative contributions between precipitation and catchment storage. It is clear that catchment storage is comparable to precipitation at monthly scale, is less comparable to precipitation at seasonal scales, and least comparable to precipitation at annual scale. At annual scale, precipitation is the dominant contributor (which means the relative contribution is largest among the three variables) of streamflow variability, with relative contribution (RC) more than 50% for 77.2% of catchments for the 15 approaches. The contributions of catchment storage (RC < 50% for 2.5% of catchments) are largely equivalent to potential evaporation (RC<50% for 2.1% of catchments). At monthly scale, catchment subsurface storage is the largest contributor at a large fraction of catchments, with RC > 50% for 30.9% of catchments. The contribution of precipitation is relatively

smaller than that at the annual scale with RC > 50% for 47.6% of catchments. The impact of potential evaporation is small for most catchments. The contributions assessed at seasonal scale are in between those at monthly and annual scales, with catchment storage having RC > 50% for 17.3% of catchments and precipitation with RC > 50% for 61.7% of catchments.

Figure S7 summarises the relative contribution among the three factors (precipitation, catchment storage and potential evaporation) for different climate regimes. It is clear that the contribution of catchment storage is stronger in water-limited regions (the aridity index (mean annual potential evaporation divided by mean annual precipitation) >1.35) than that in energy-limited regions (wet/cold regions with aridity index <0.76). In comparison, the contribution of precipitation is stronger in energy-limited regions than that in water-limited regions. At monthly scale, the contribution of potential evaporation is largely similar between the energy-limited regions and water-limited regions. However, at annual scale the contribution of potential evaporation for the energy-limited regions is noticeably larger than that for water-limited regions. The behavior of the equitant regions (between the water-limited and energy-limited) is in between the two.

Figures S8–S21 support the findings from Figure 5, but show more comprehensive results from 14 out of 15 approaches using catchment storage and potential evaporation (except for one approach that uses Lyne-Hollick storage and Penman potential evaporation). All 14 approaches show similar spatial patterns.

Figures S22–S28 repeat Figures S2-S8, respectively. All the results shown in Figures S23–S29 are generated from groundwater recharge simulated from four global hydrological models together with their forcing data of precipitation and potential evaporation in 1628 catchments. There are 4 combinations for the four global hydrological models, respectively. The results support the findings that the global models can work similarly at annual and seasonal scales, but much worse at monthly scales (Figures S22–S23). Furthermore, using the global model results cannot identify the increasing pattern of precipitation elasticity and the decreasing pattern of storage elasticity from monthly to annual scales (Figure S24–S28).

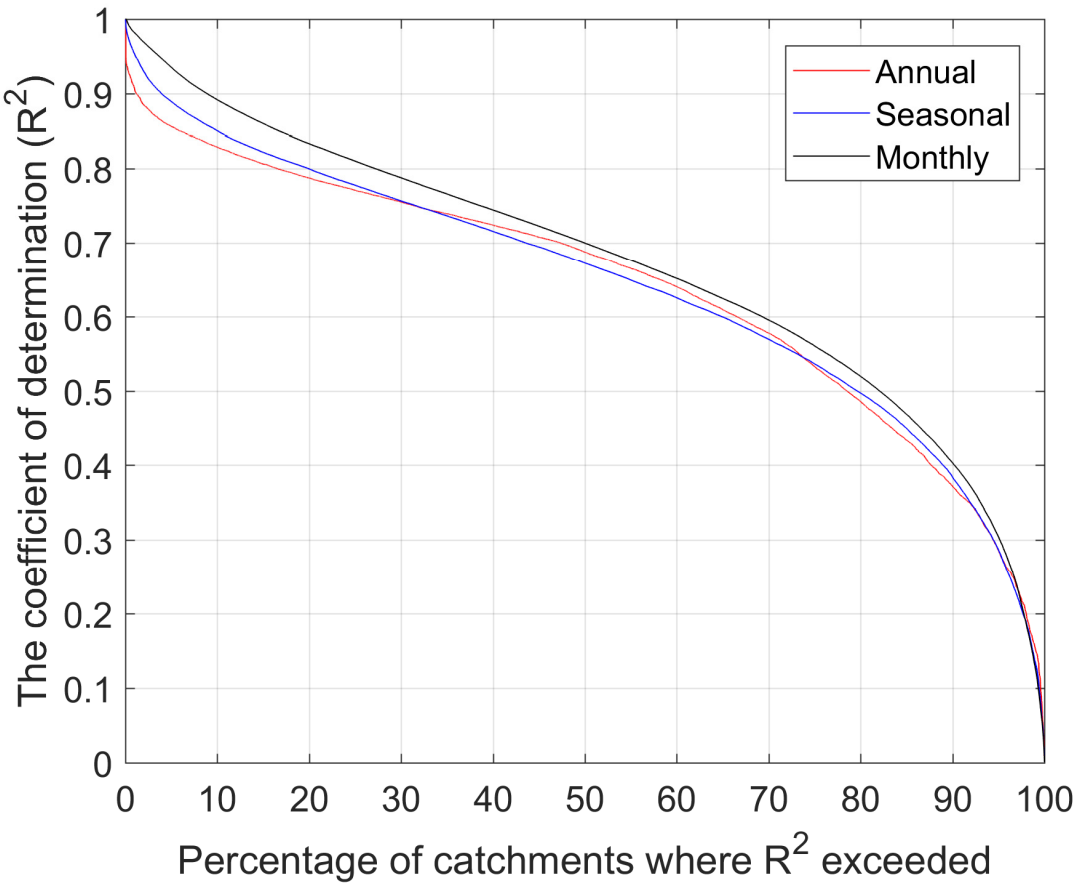

Figure S1. Summary of the performance of the multi-temporal framework for attributing streamflow variation in all 1628 catchments, for each of the 15 approaches used.

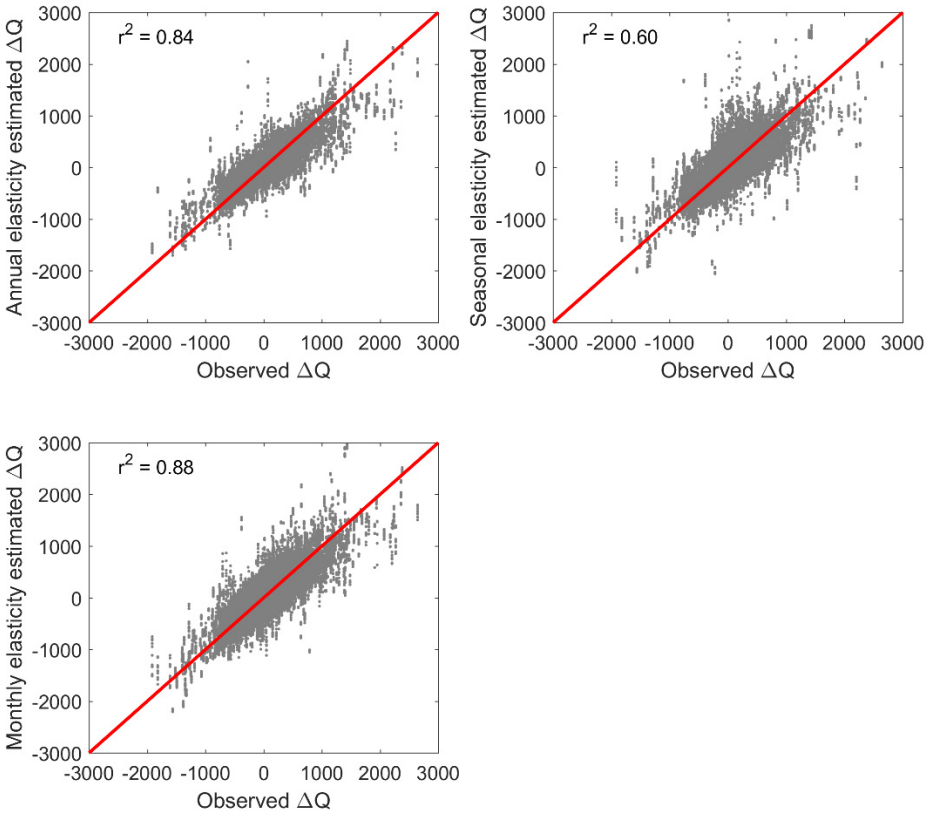

Figure S2. Comparisons of observed annual streamflow variability (ΔQ, in mm/year) with that estimated (mm/year) from all three drivers (precipitation, groundwater storage and potential evaporation) and at three temporal scales (annual, seasonal and monthly). The ΔQ_i is taken as the sum of $\Delta Q_{i,j}$ where i is for the i^{th} year and j is for the j^{th} month (or season) (see Equation (2)). Data are obtained from all 1628 catchments and 15 approaches.

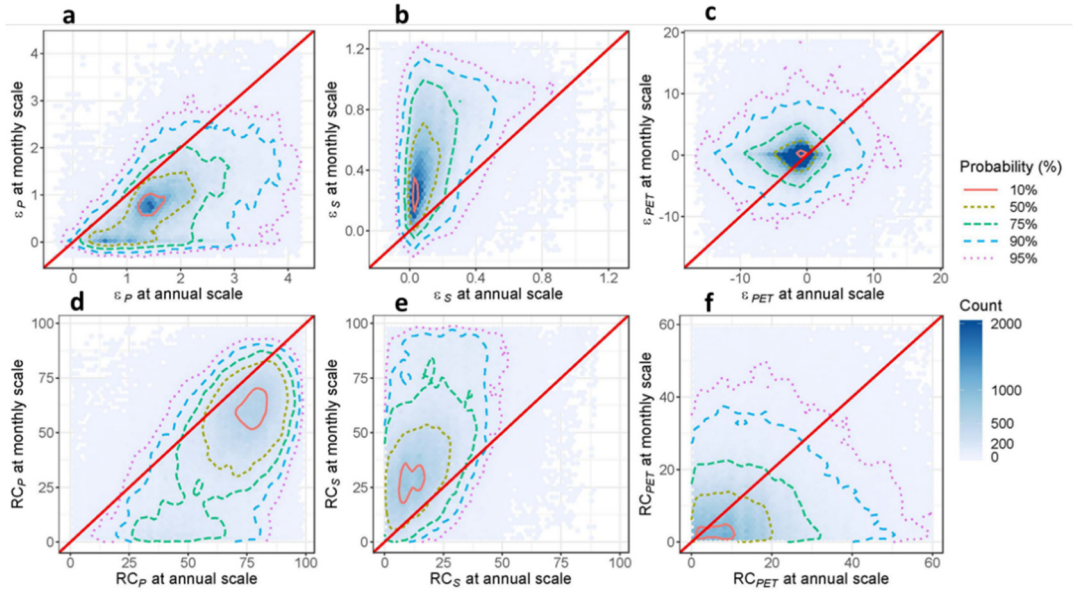

Figure S3. Comparisons of streamflow elasticity between monthly and annual scales and comparisons of the relative contributions of the three variables obtained from 15 methods. (**a**). Precipitation elasticity of streamflow (ϵ_P) between monthly and annual scales. (**b**). Groundwater storage elasticity of streamflow (ϵ_S) between monthly and annual scales. (**c**). Potential evaporation elasticity of streamflow (ϵ_{PET}) between monthly and annual scales. (**d**). Relative contribution of precipitation between monthly and annual scales. (**e**). Relative contribution of groundwater storage between monthly and annual scales. (**f**). Relative contribution of potential evaporation between monthly and annual scales. Each closed contour indicates the probability of occurrence of the variables being compared in (**a**–**f**).

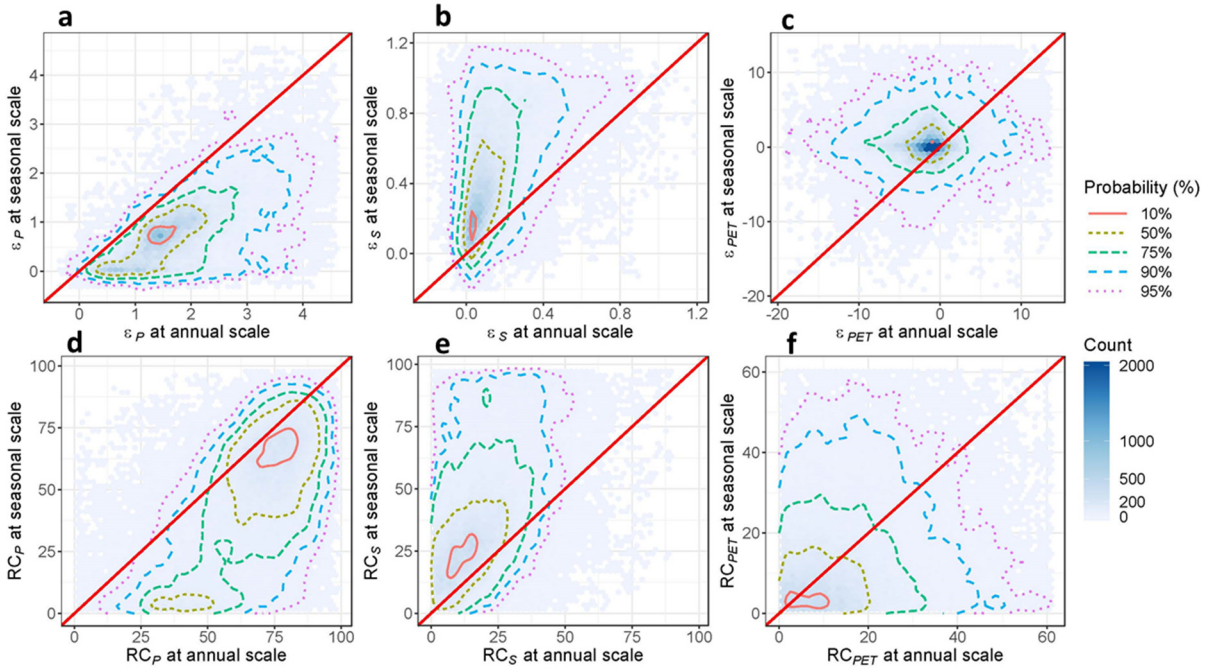

Figure S4. Same as Figure S3, but for the comparisons between seasonal and annual scales.

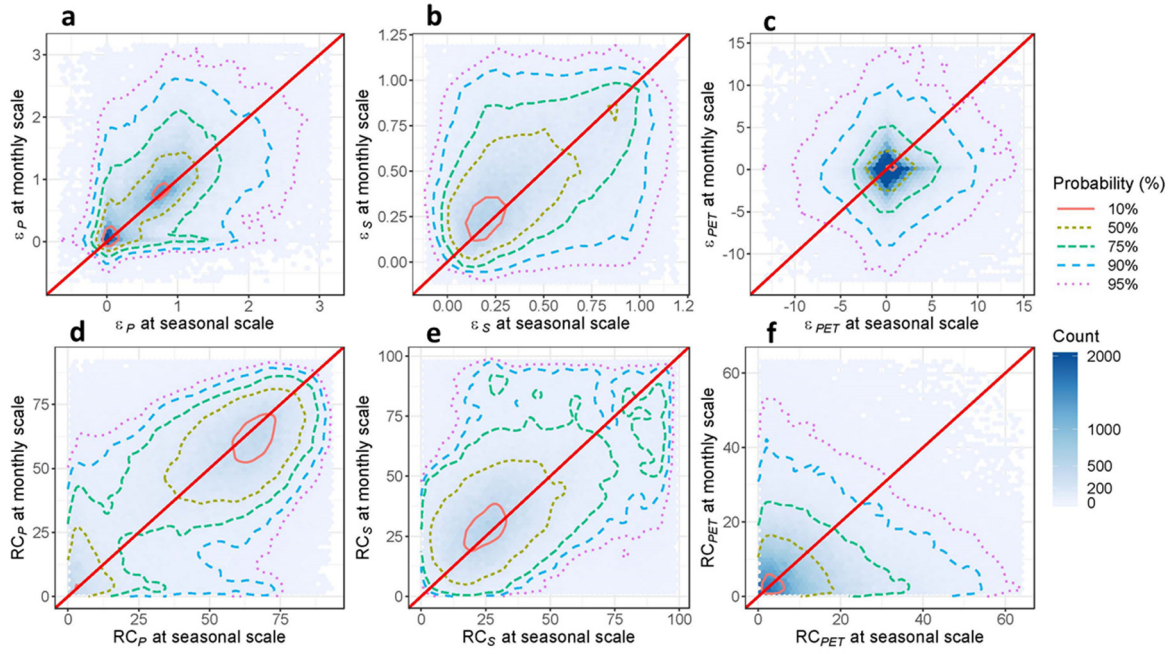

Figure S5. Same as Figure S3, but for the comparisons between monthly and seasonal scales.

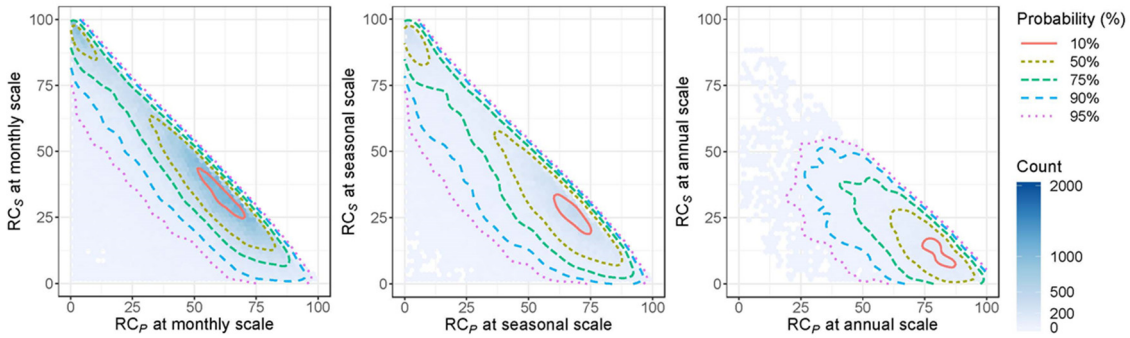

Figure S6. Comparisons between relative contribution of catchment storage (*RCs*) and relative contribution of precipitation (RC_p) at three temporal scales: monthly, seasonal and annual.

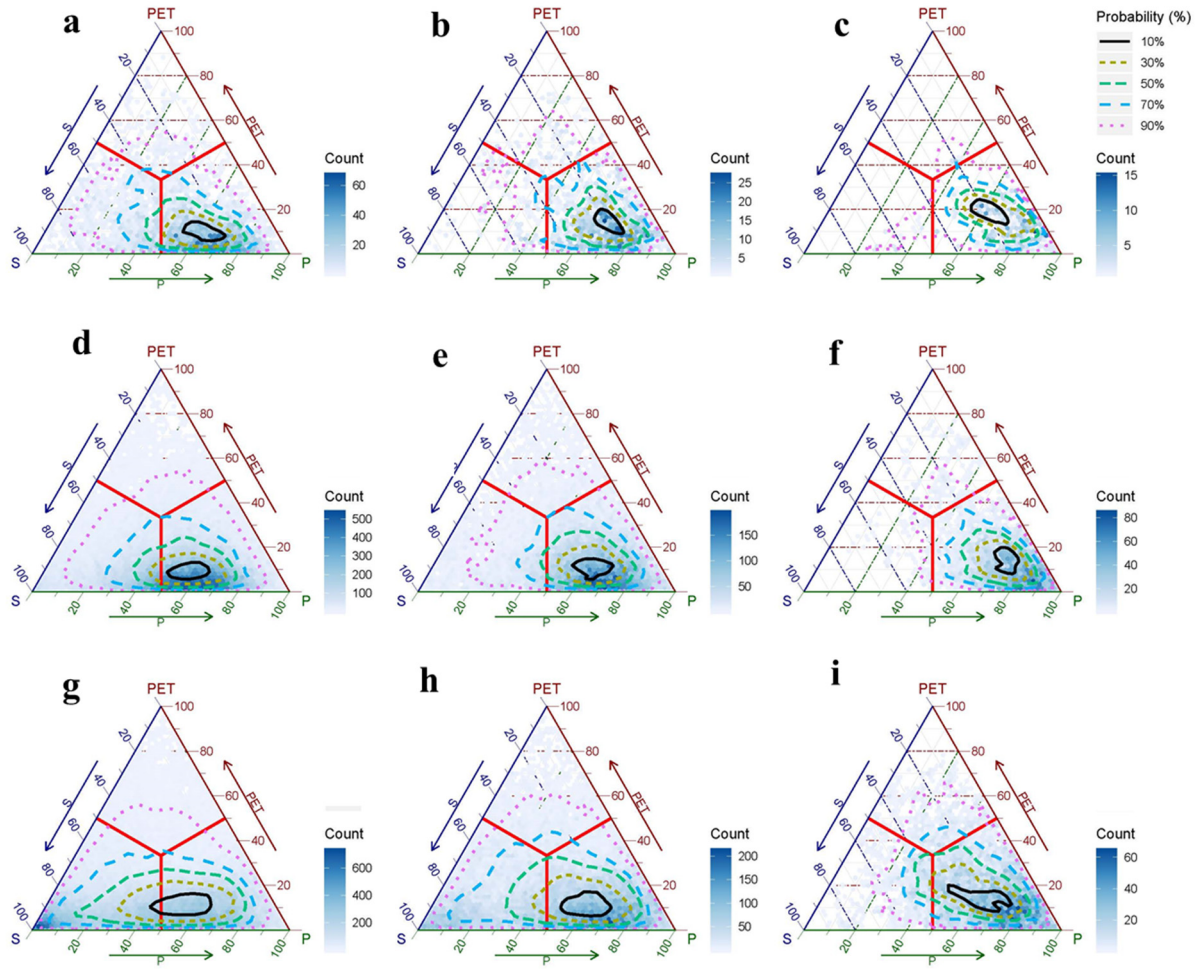

Figure S7. Relative contribution (%) of precipitation (*P*), groundwater storage (*S*) and potential evaporation (*PET*) to streamflow variability at monthly (**a**,**d**,**g**), seasonal (**b**,**e**,**h**) and annual (**c**,**f**,**i**) scales for different climate regimes (top three panels (**a**–**c**) for energy-limited, middle three panels (**d**–**f**) for equitant, bottom three panels (**g**–**i**) for water-limited) and for all combinations of catchments and approaches (1268 catchments × 15 approaches). The space enclosed by the contours correspond to 10%, 30%, 50%, 70% and 90% probability. The number of points (count) is indicated using a filled color in each hexagon bin. The sum of the three contributions equals to 100%.

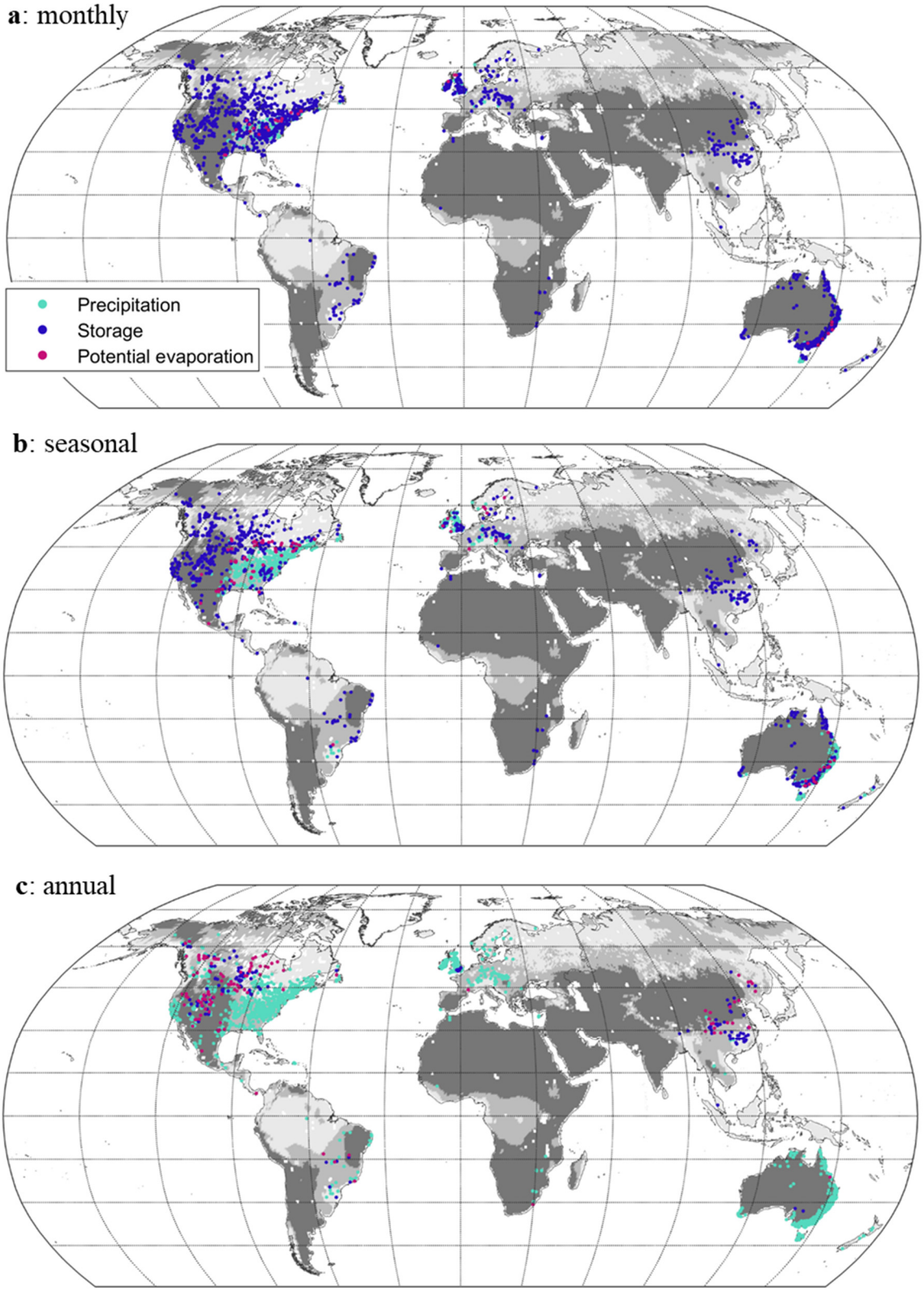

Figure S8. The largest contribution factor to the streamflow variability. (**a**) monthly scale. (**b**) seasonal scale. (**b**) annual scale. Cyan, blue and red are for precipitation, storage and potential evaporation, respectively. Energy-limited (aridity index, AI < 0.76), equitant (0.76 ≤ AI ≤1.35) and water-limited (AI >1.35) regions are represented by light grey, grey, and dark grey. The results is obtained from one approach that uses Boughton-Chapman storage and Penman potential evaporation.

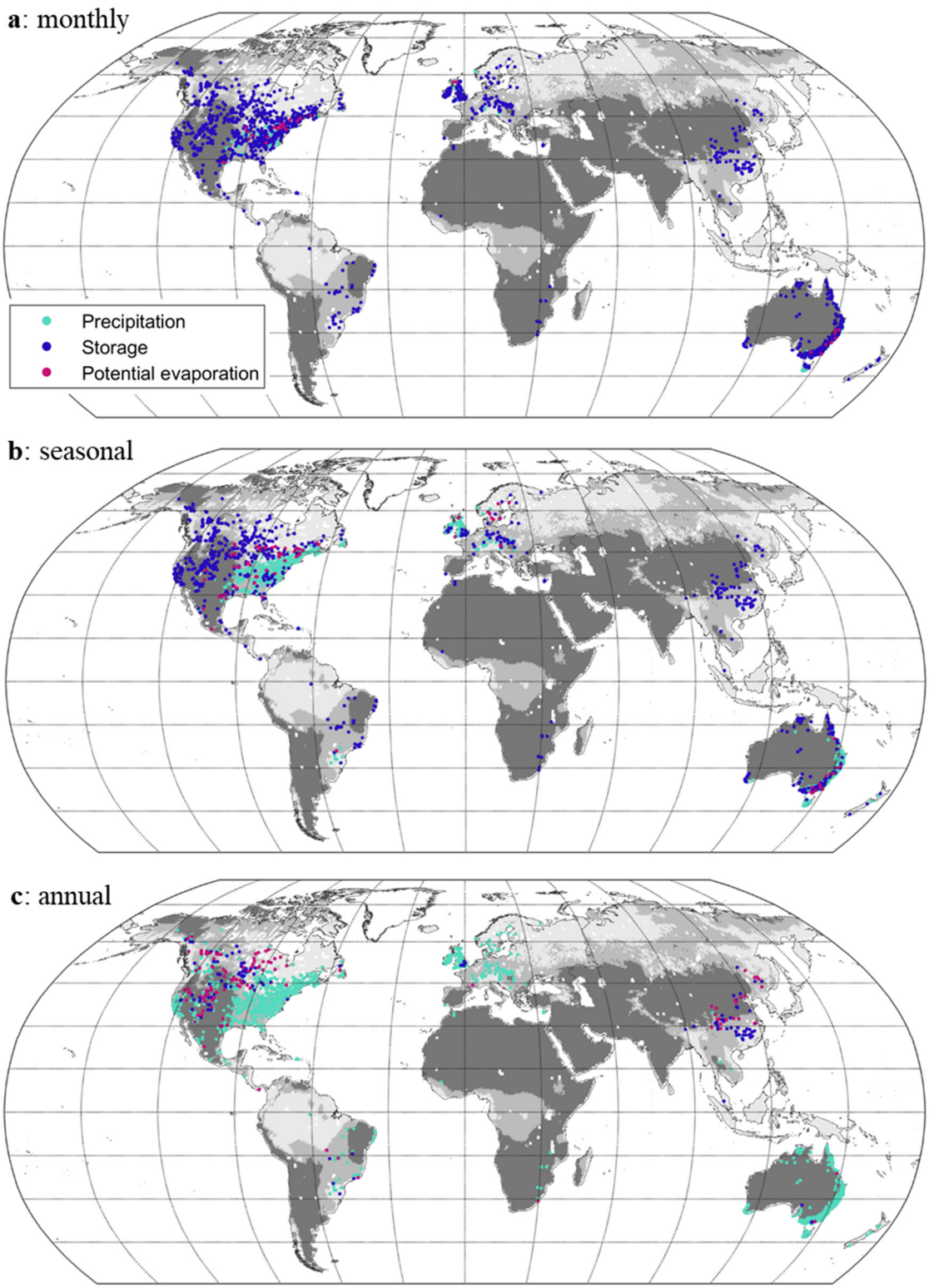

Figure S9. Same as Figure S8, but obtained from the method using Chapman-Maxwell storage and Penman potential evaporation.

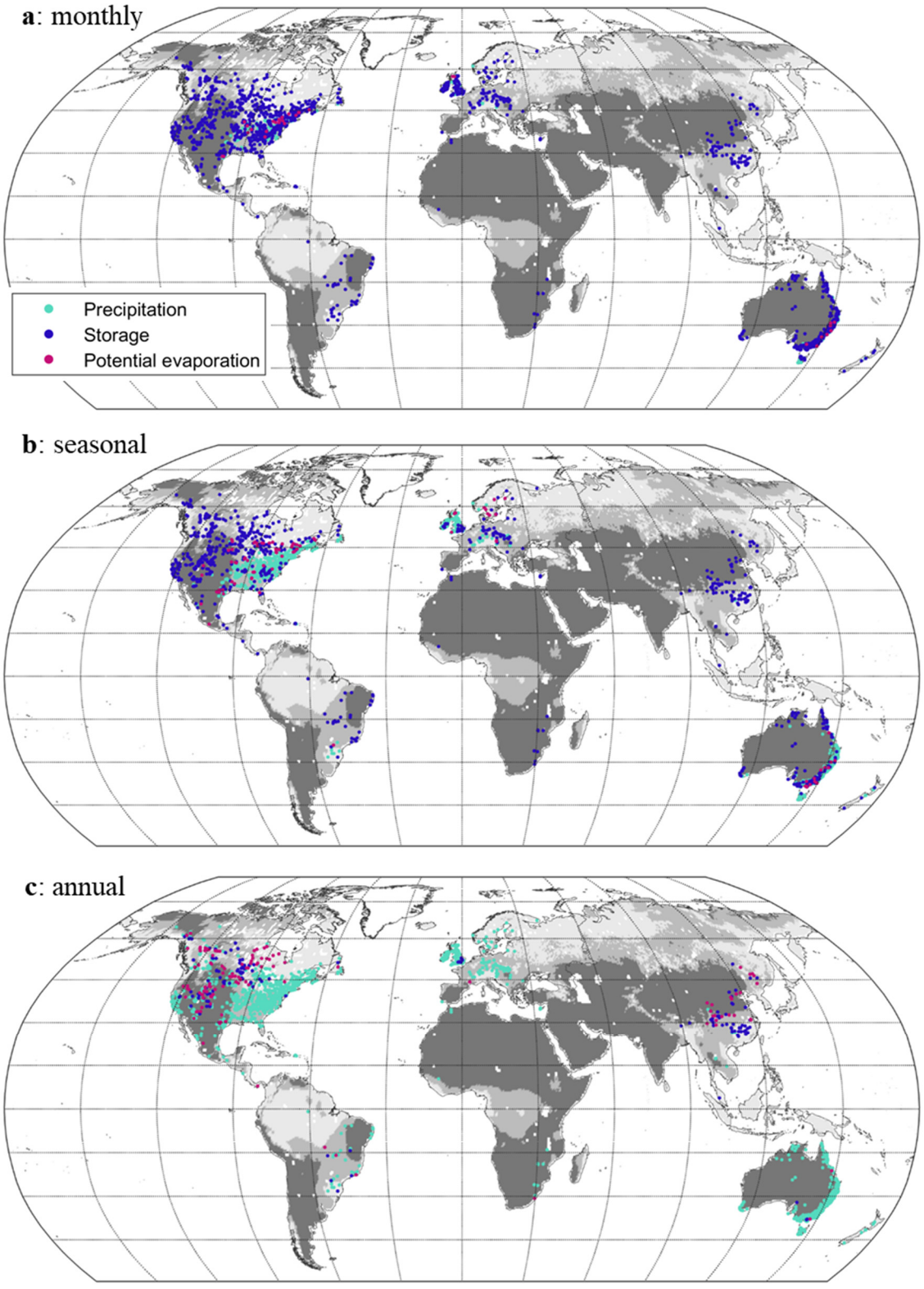

Figure S10. Same as Figure S8, but obtained from the method using Eckhard storage and Penman potential evaporation.

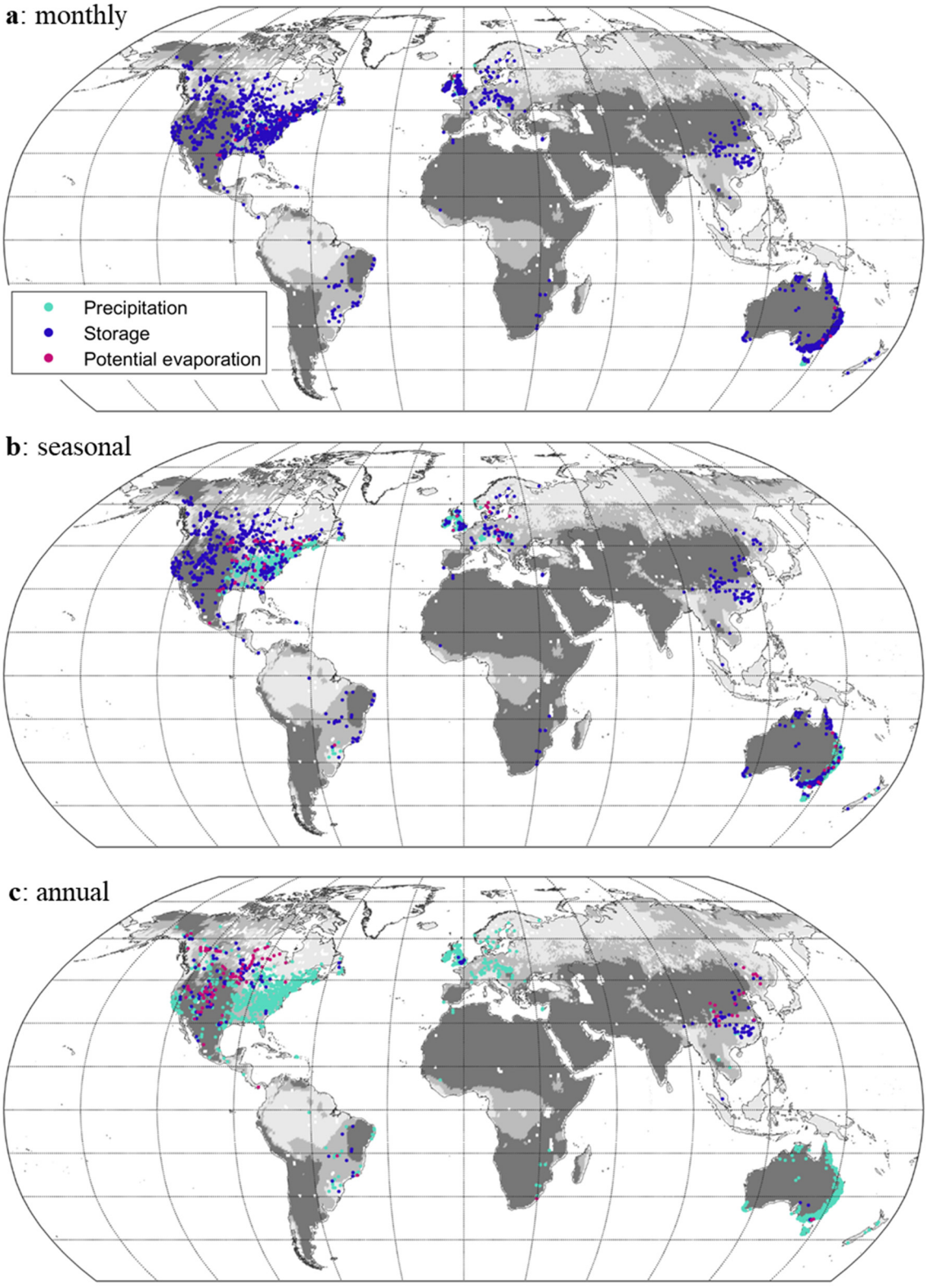

Figure S11. Same as Figure S8, but obtained from the method using Standard storage and Penman potential evaporation.

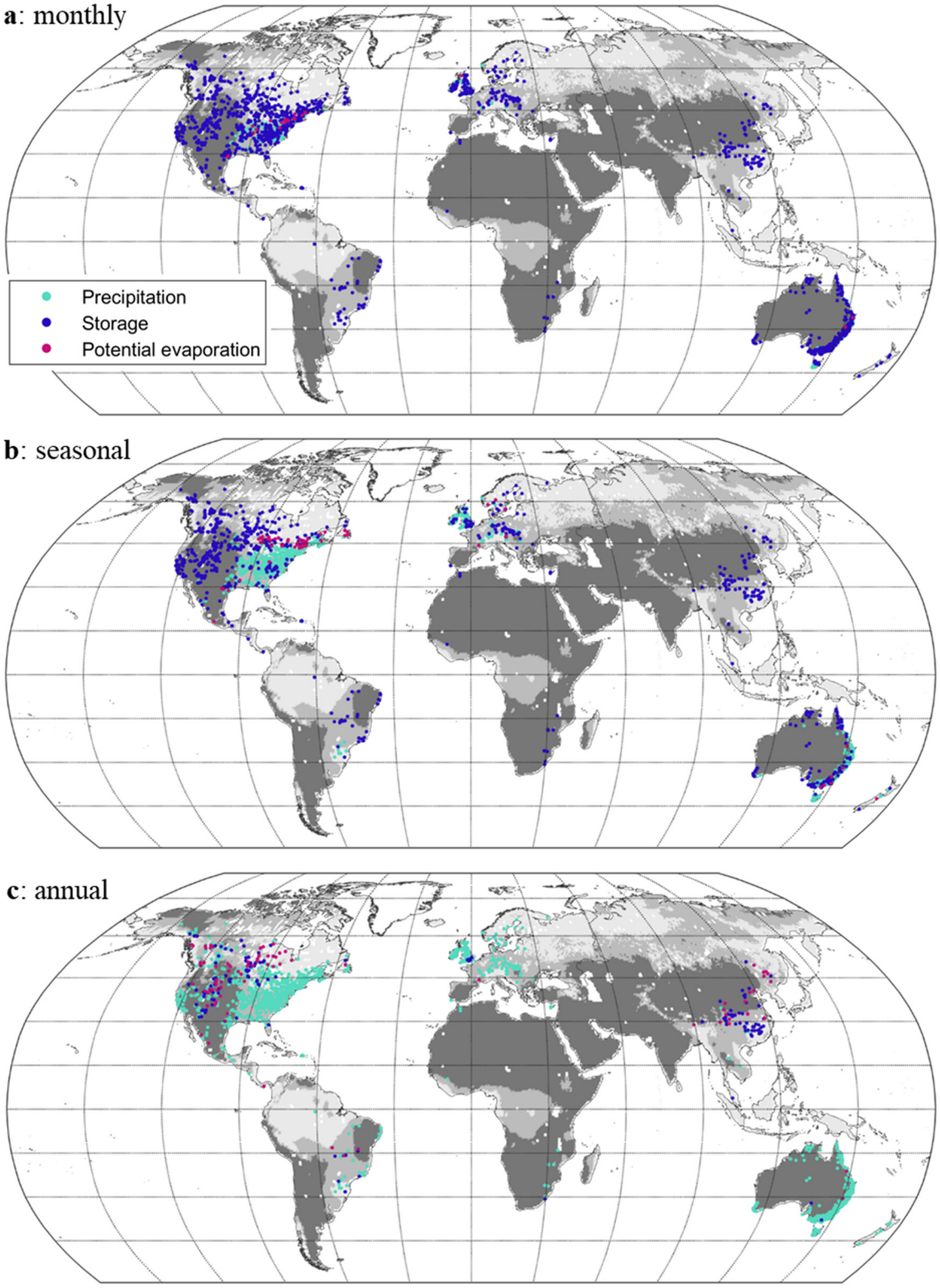

Figure S12. Same as Figure S8, but obtained from the method using Boughton-Chapman storage and Priestley-Taylor potential evaporation.

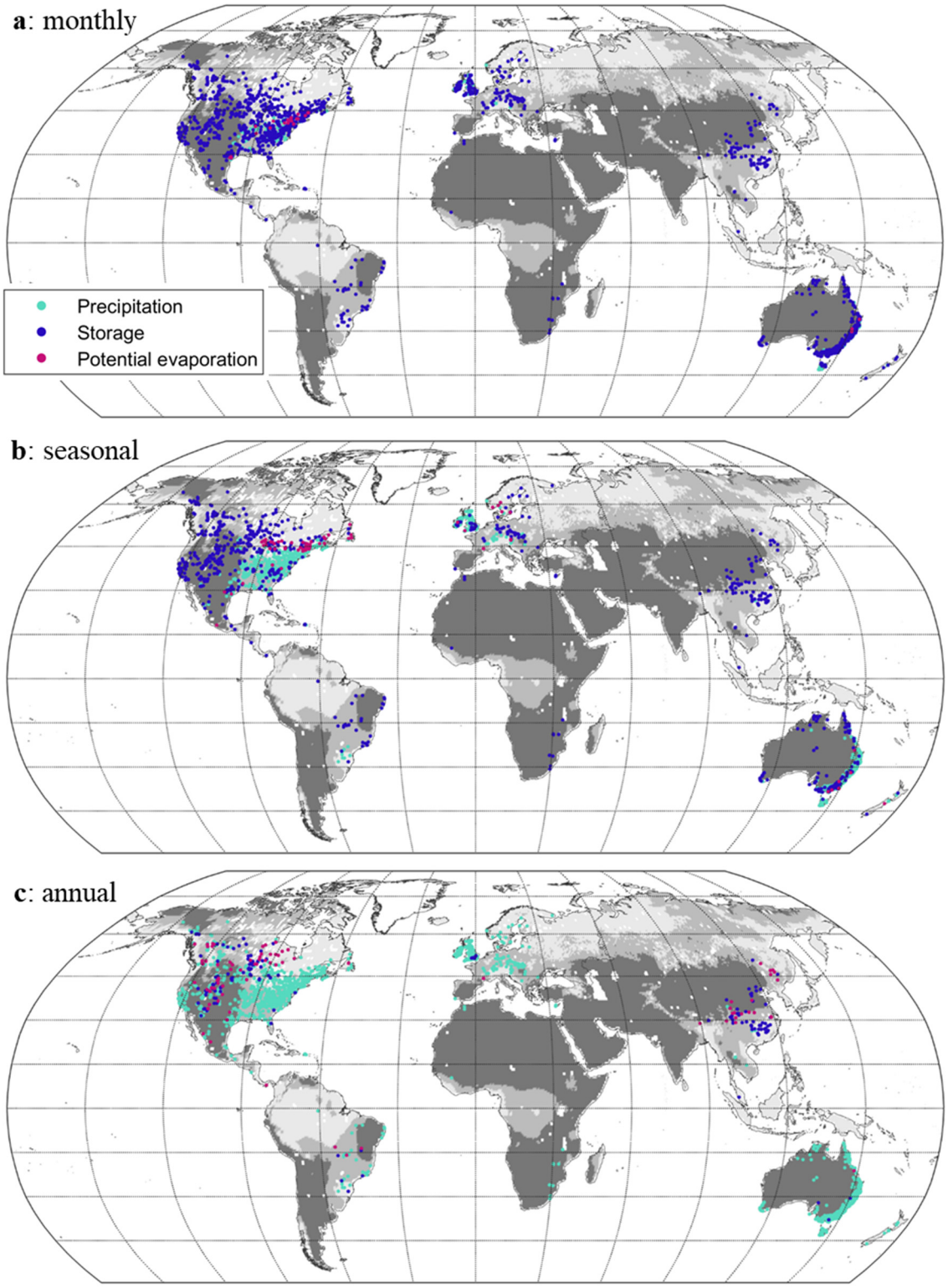

Figure S13. Same as Figure S8, but obtained from the method using Chapman-Maxwell storage and Priestley-Taylor potential evaporation.

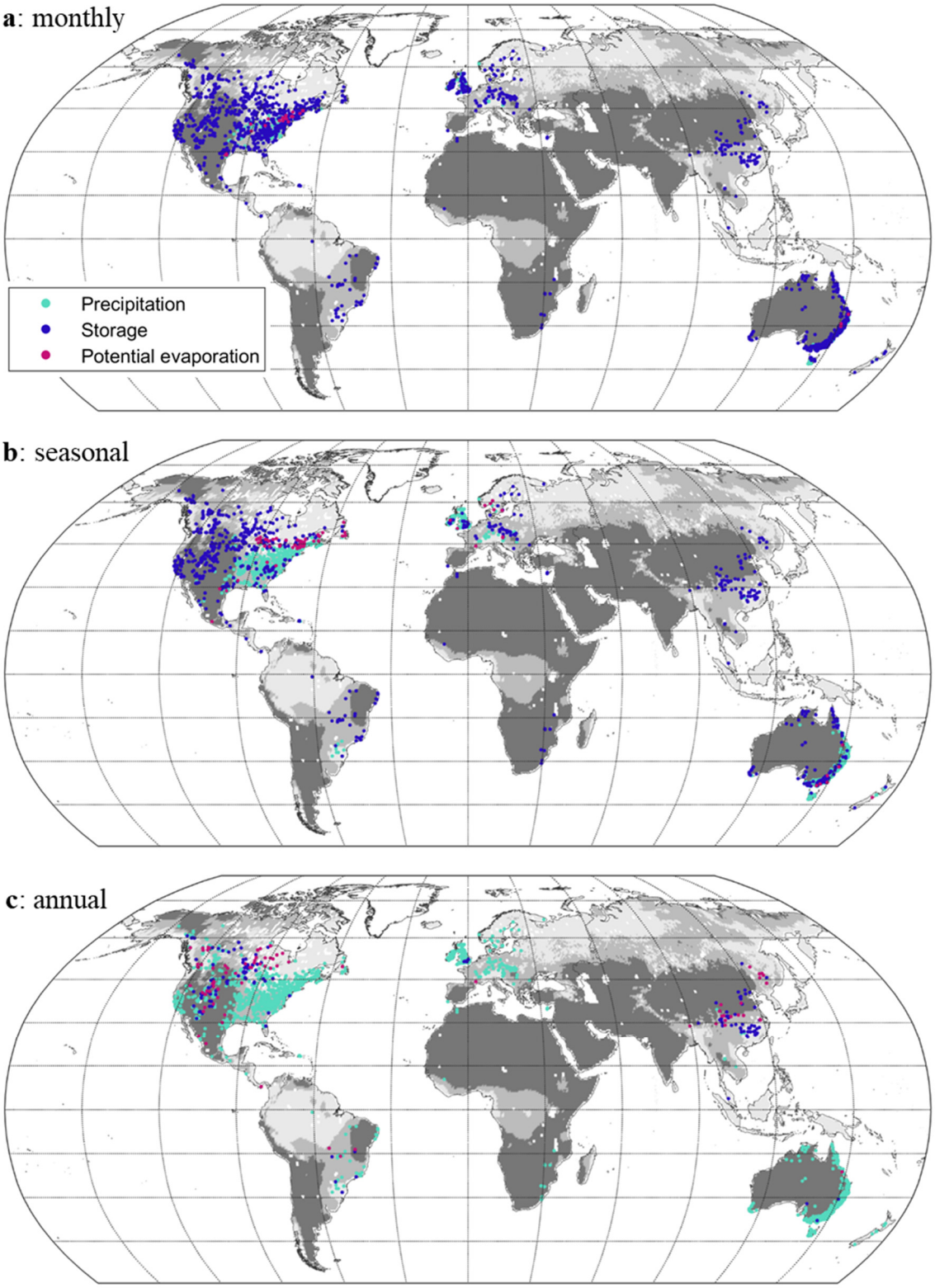

Figure S14. Same as Figure S8, but obtained from the method using Eckhard storage and Priestley-Taylor potential evaporation.

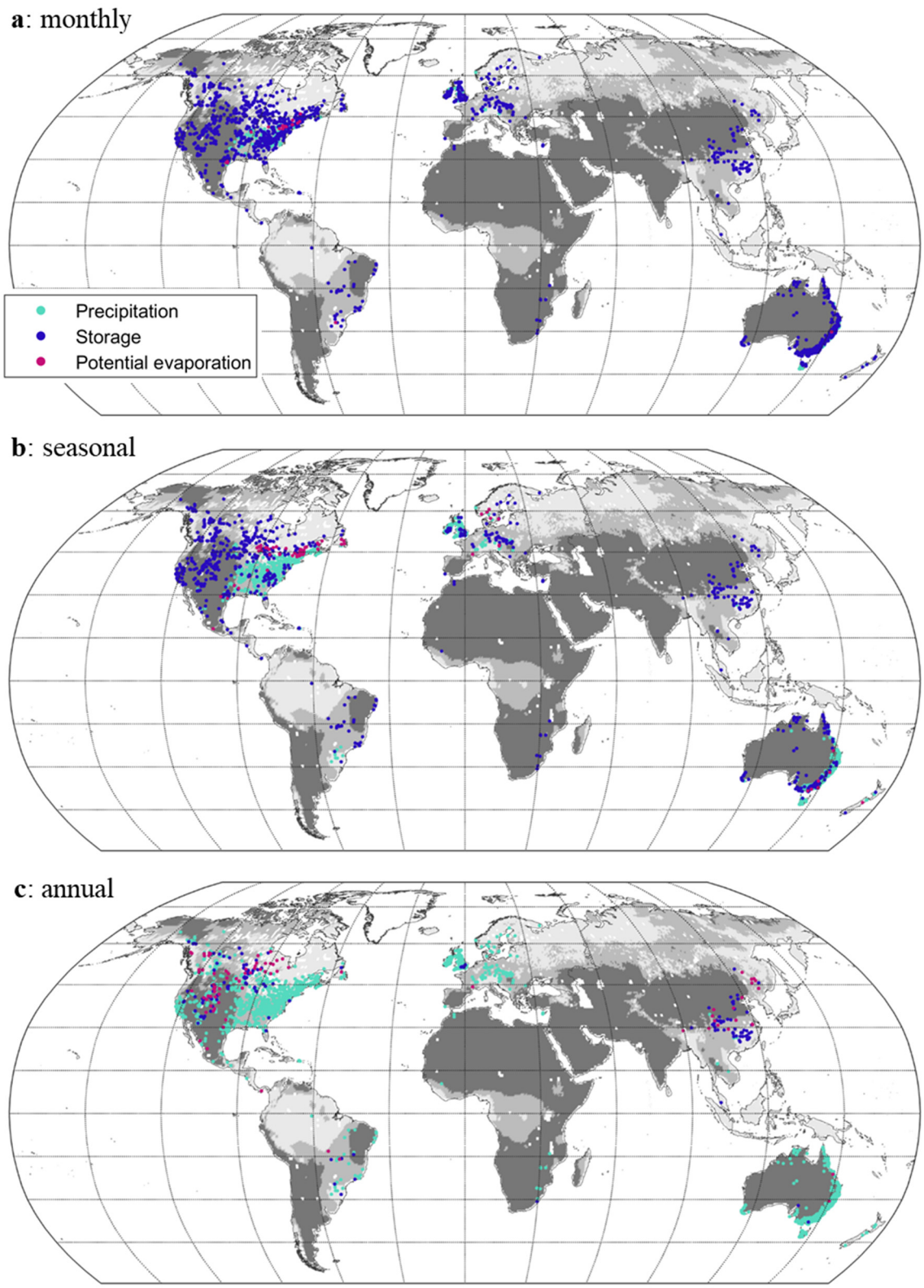

Figure S15. Same as Figure S8, but obtained from the method using Lyne-Hollick storage and Priestley-Taylor potential evaporation.

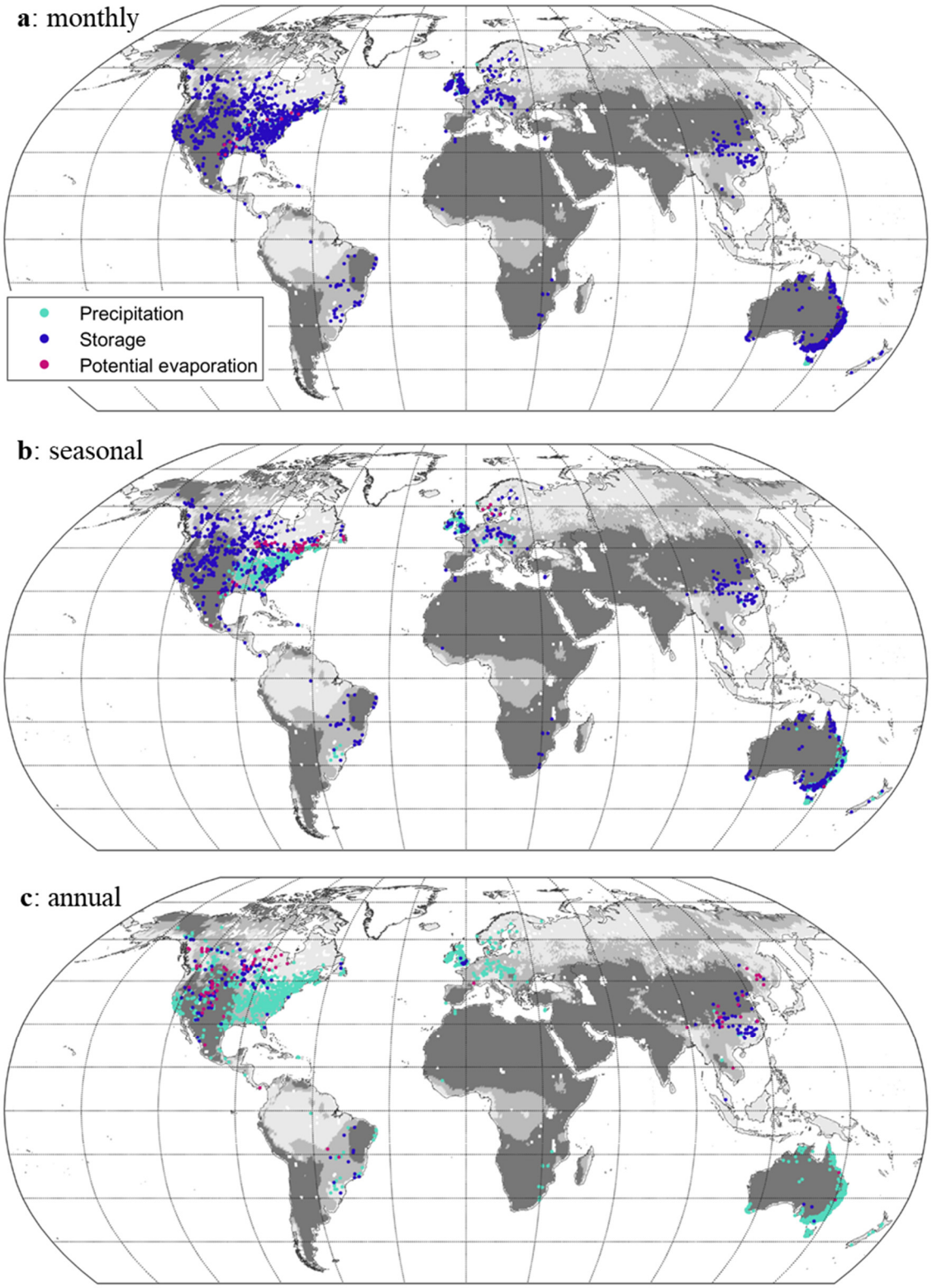

Figure S16. Same as Figure S8, but obtained from the method using Standard storage and Priestley-Taylor potential evaporation.

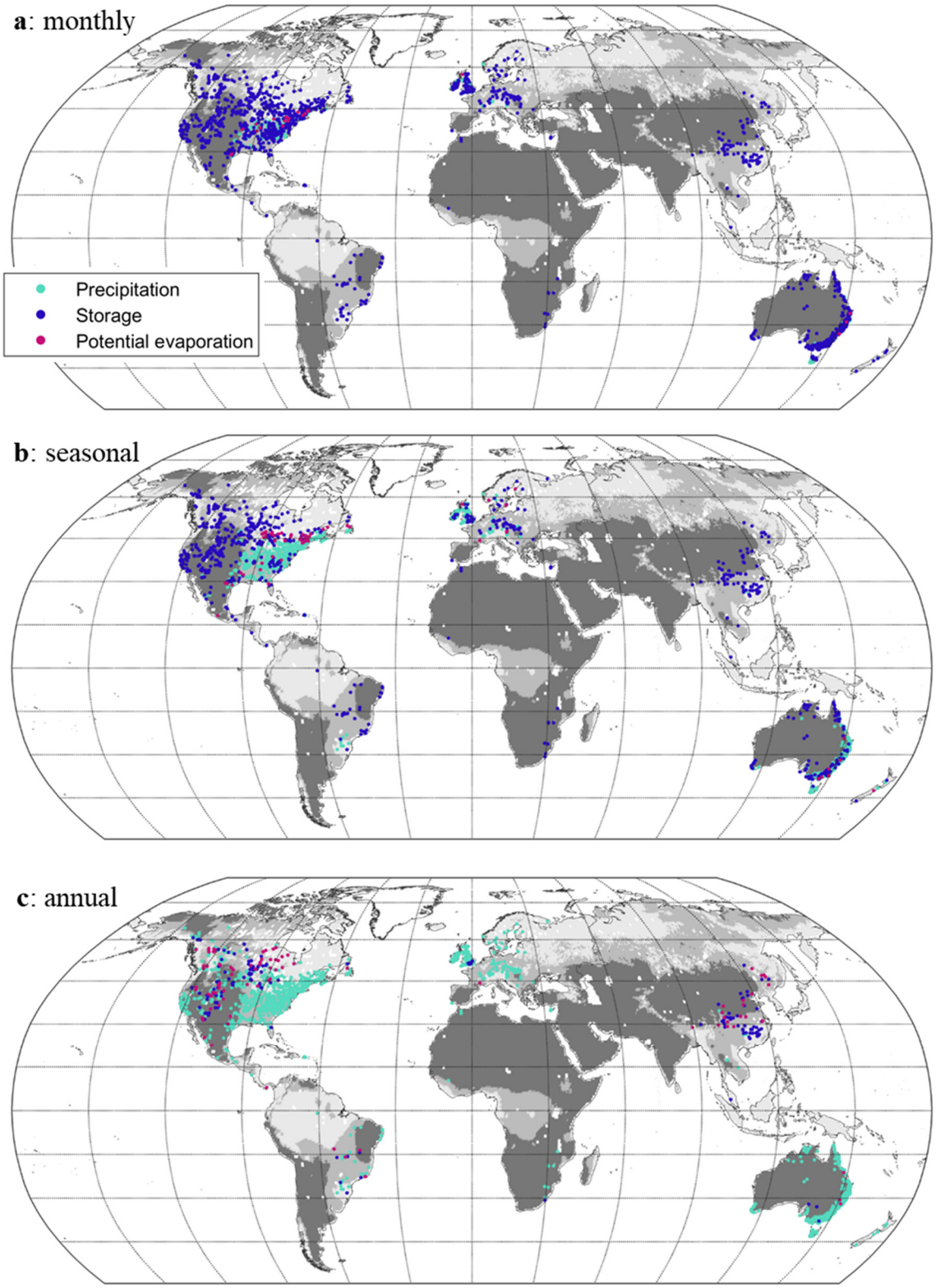

Figure S17. Same as Figure S8, but obtained from the method using Boughton-Chapman storage and Morton potential evaporation.

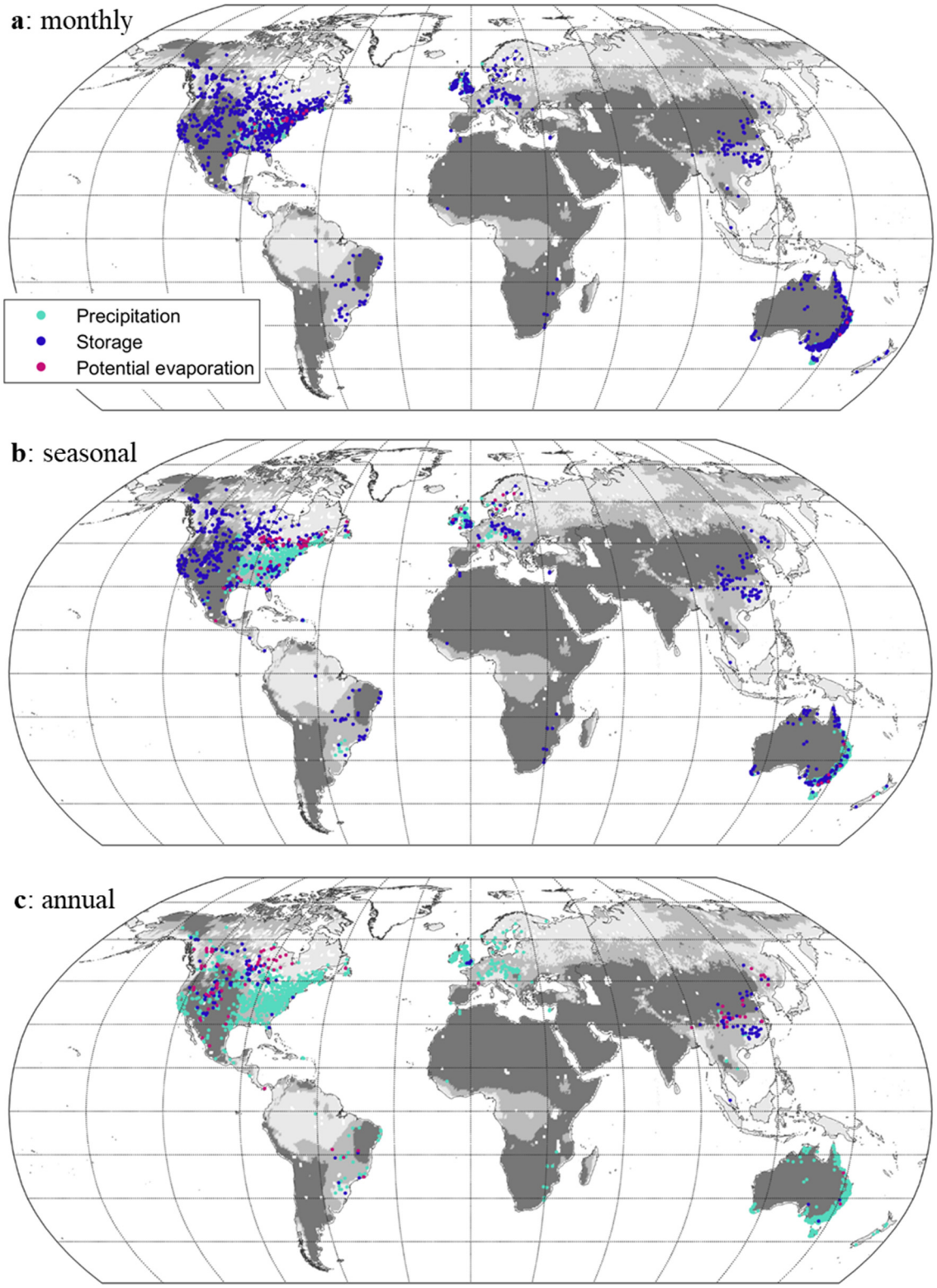

Figure S18. Same as Figure S8, but obtained from the method using Chapman-Maxwell storage and Morton potential evaporation.

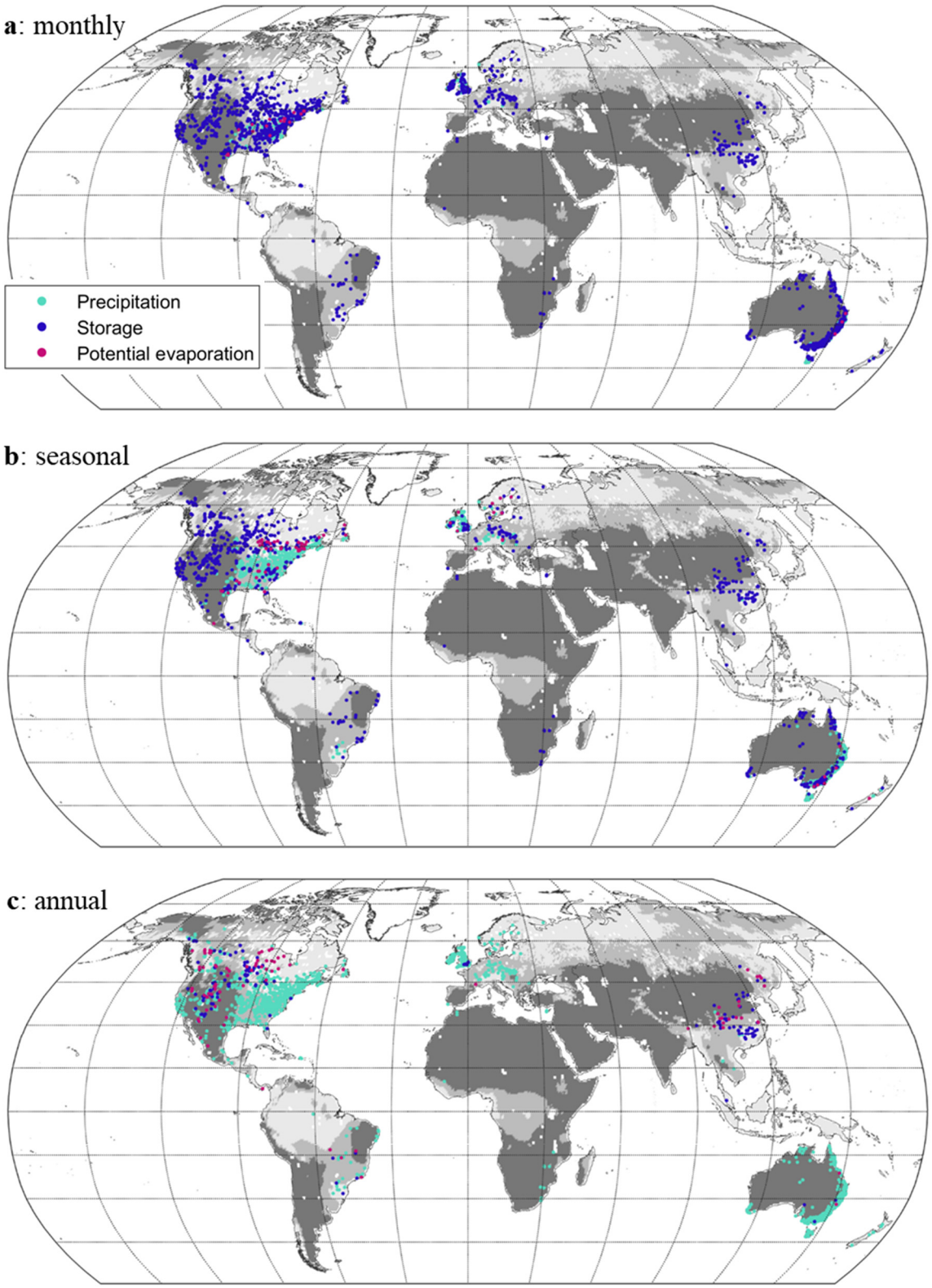

Figure S19. Same as Figure S8, but obtained from the method using Eckhard storage and Morton potential evaporation.

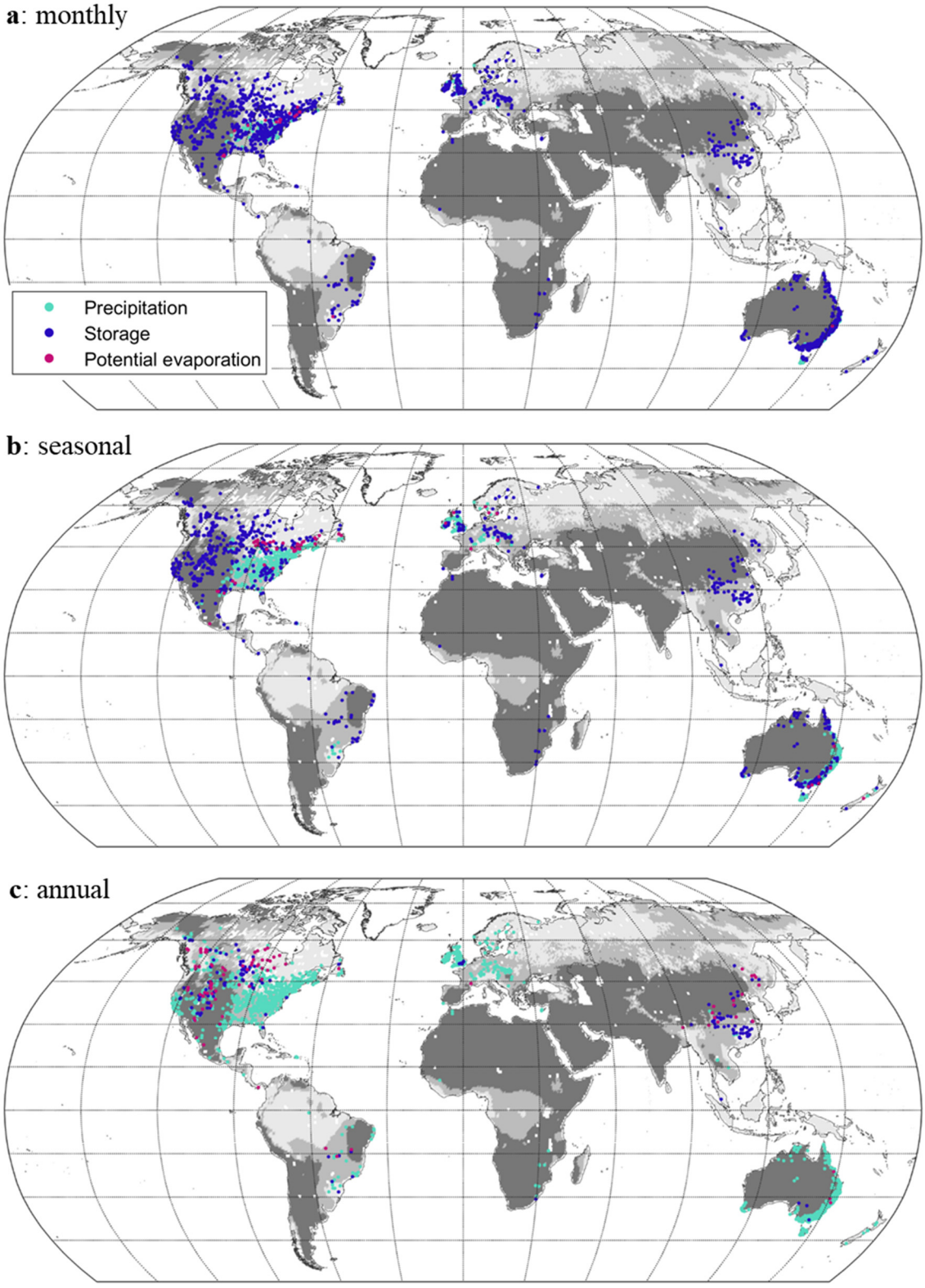

Figure S20. Same as Figure S8, but obtained from the method using Lyne-Hollick storage and Morton potential evaporation.

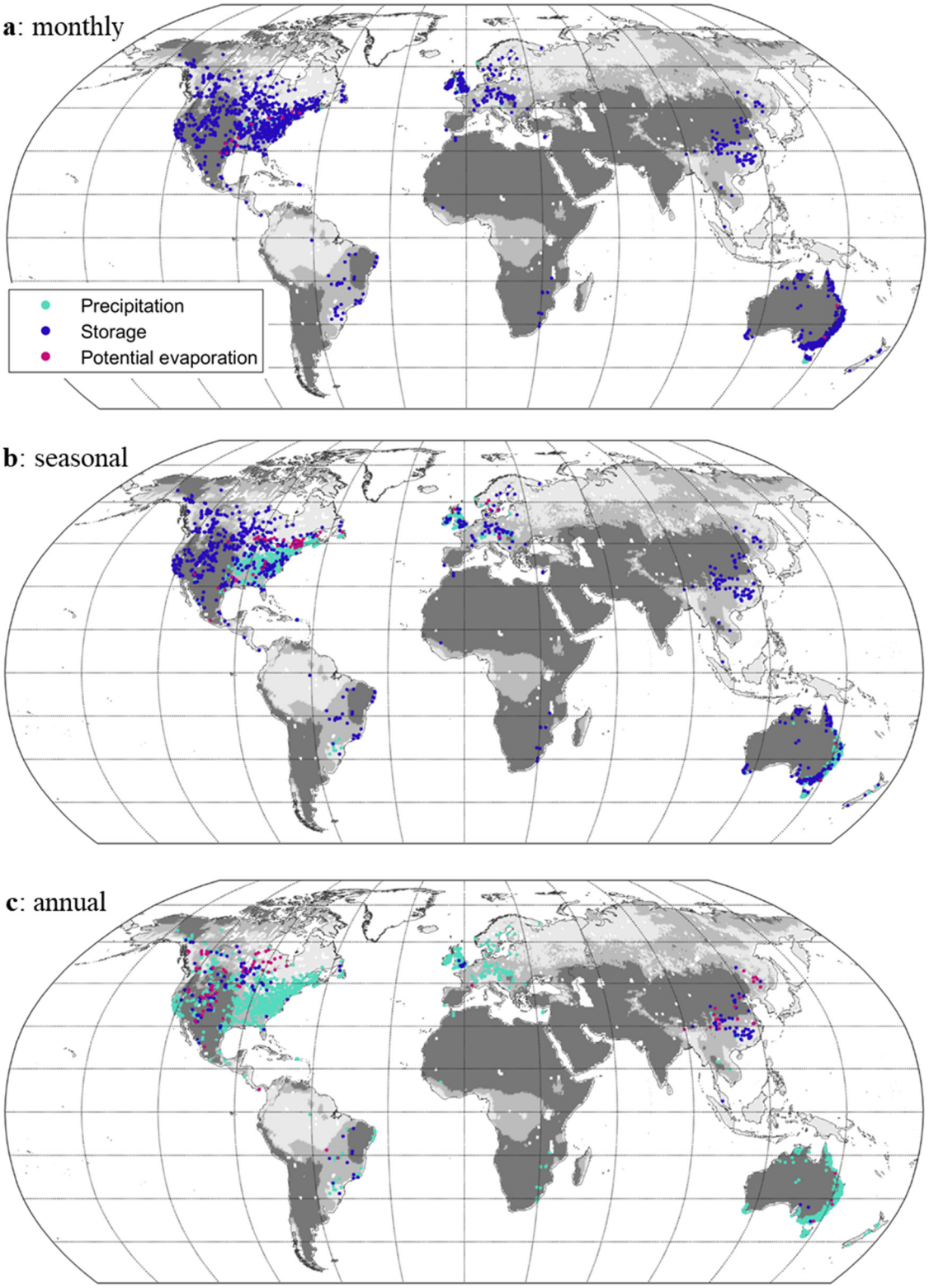

Figure S21. Same as Figure S8, but obtained from the method using Standard storage and Morton potential evaporation.

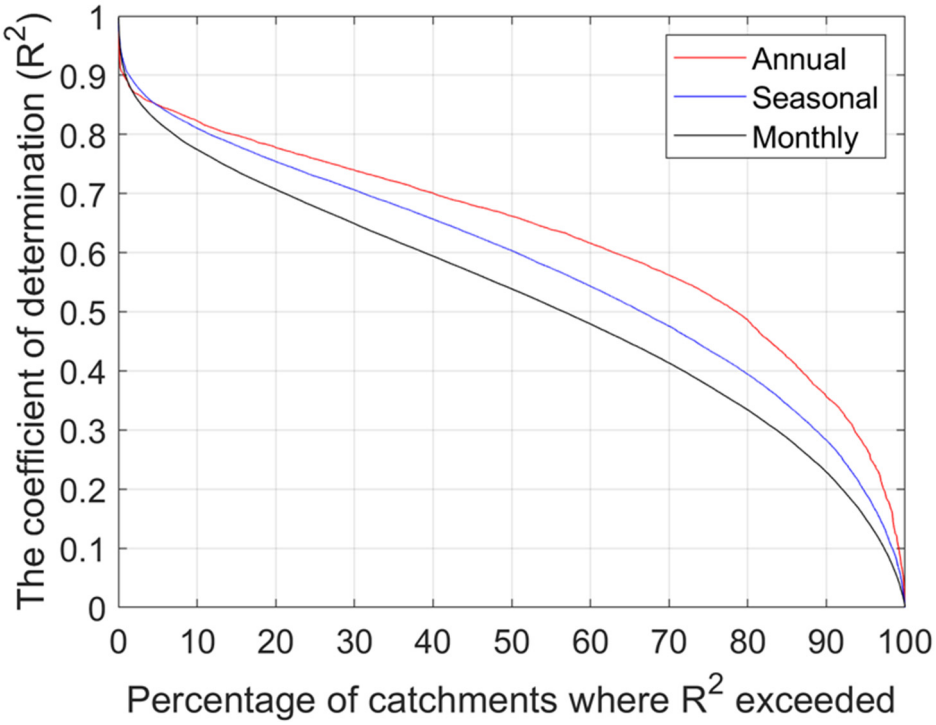

Figure S22. Same as Figure S1, but obtained from groundwater recharge simulated from four global hydrological models together with their forcing data of precipitation and potential evaporation in 1351 catchments. Note that there are 277 of 1628 catchments without the global hydrological model outputs and therefore they were eliminated for the analysis.

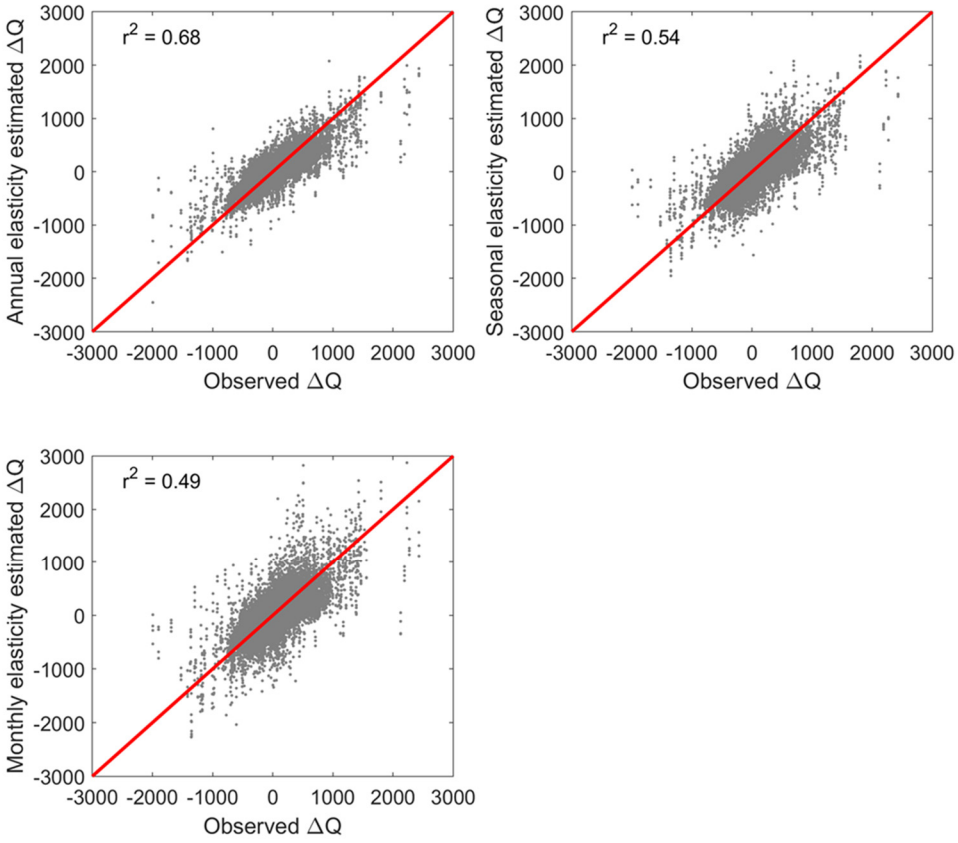

Figure S23. Same as Figure S2, but ΔQ obtained from groundwater recharge simulated from four global hydrological models together with their forcing data of precipitation and potential evaporation in 1351 catchments. There are total of 4 combinations obtained from the four global hydrological models.

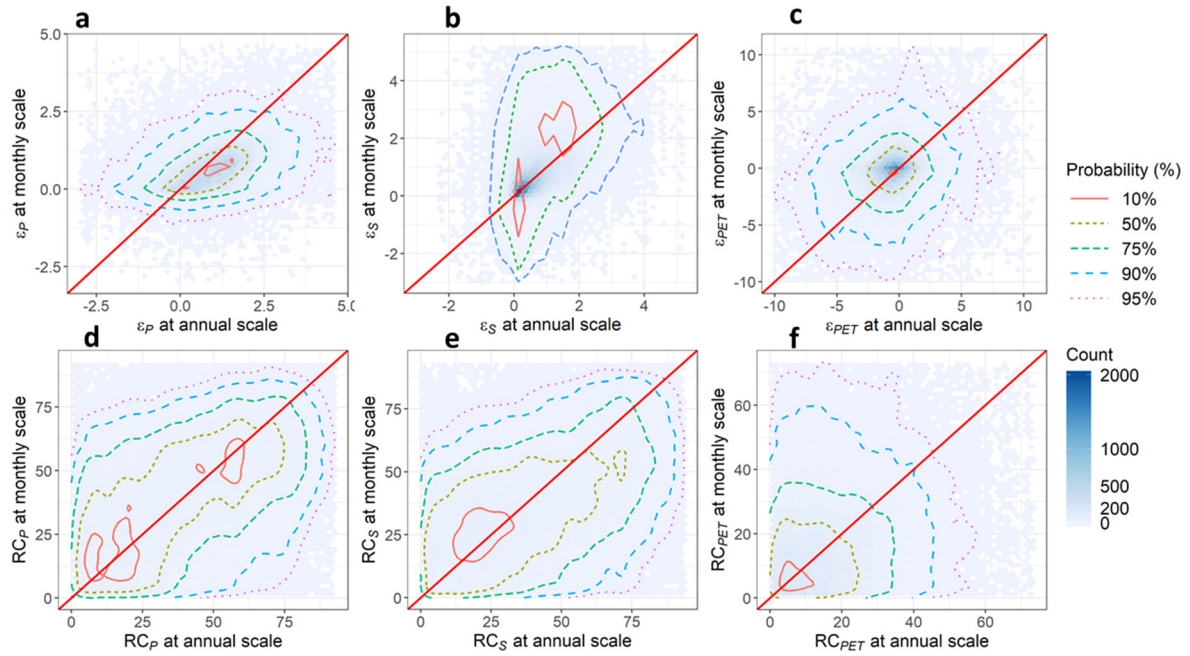

Figure S24. Same as Figure S2, but the elasticity obtained from groundwater recharge simulated from four global hydrological models together with their forcing data of precipitation and potential evaporation in 1351 catchments. There are total of 4 combinations obtained from the four global hydrological models.

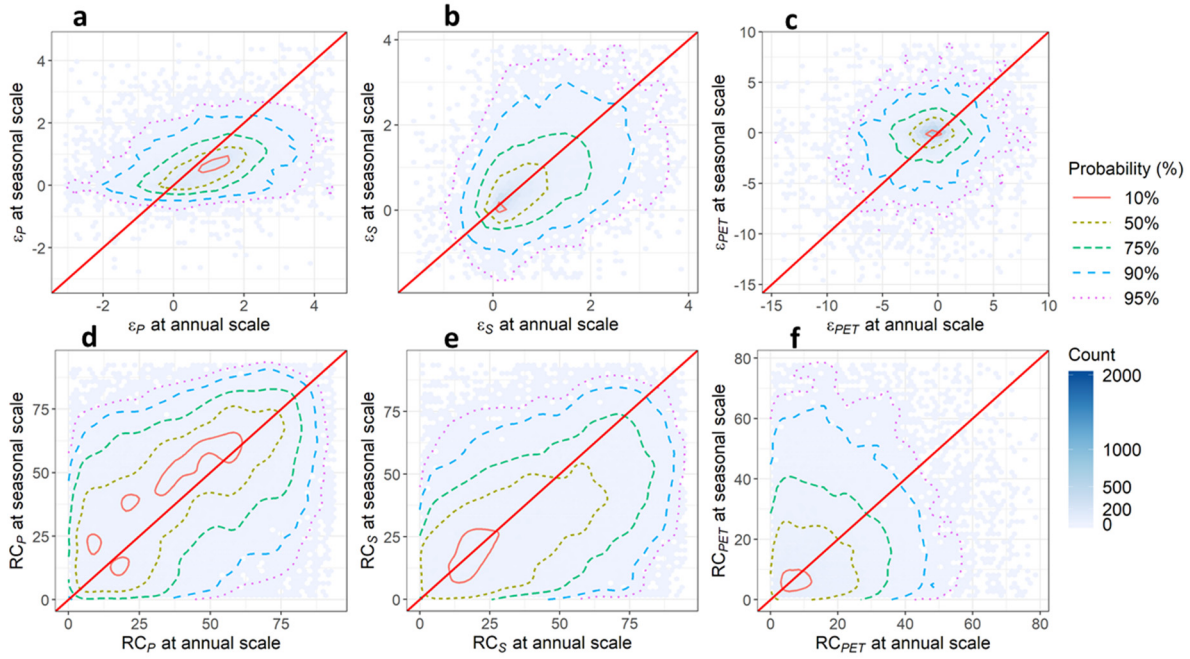

Figure S25. Same as Figure S24, but for the comparisons between seasonal and annual scales.

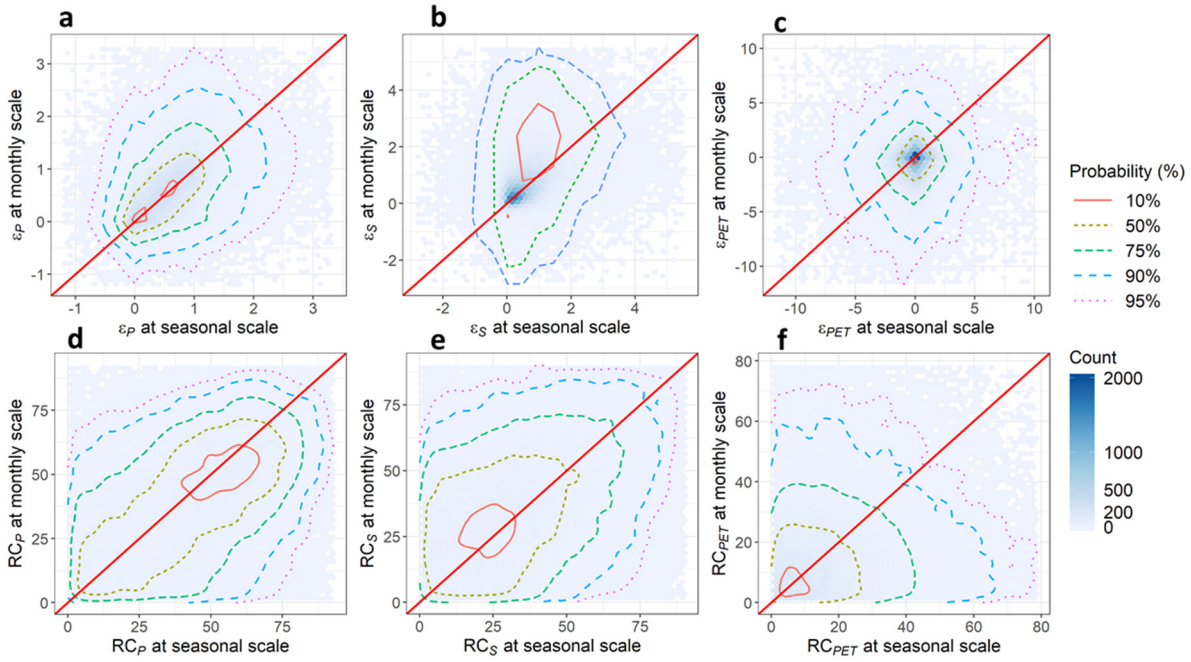

Figure S26. Same as Figure S24, but for the comparisons between monthly and seasonal scales.

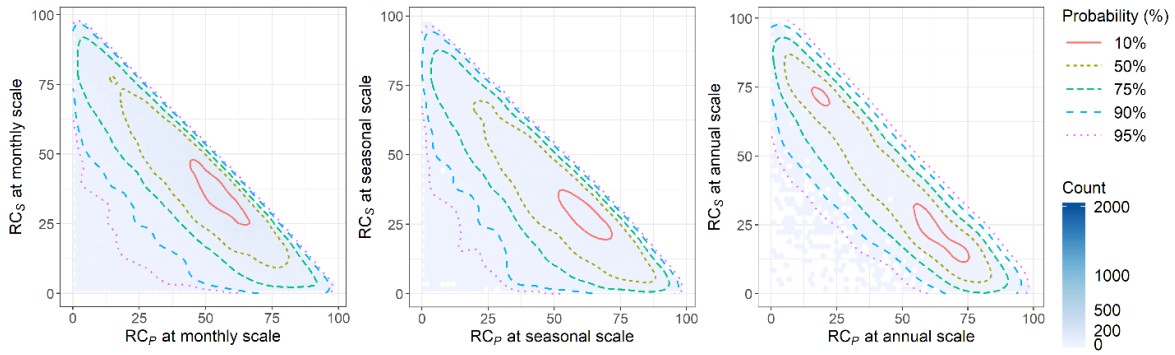

Figure S27. Same as Figure S6, but the relative contributions obtained from groundwater recharge simulated from four global hydrological models together with their forcing data of precipitation and potential evaporation in 1351 catchments. There are total of 4 combinations obtained from the four global hydrological models.

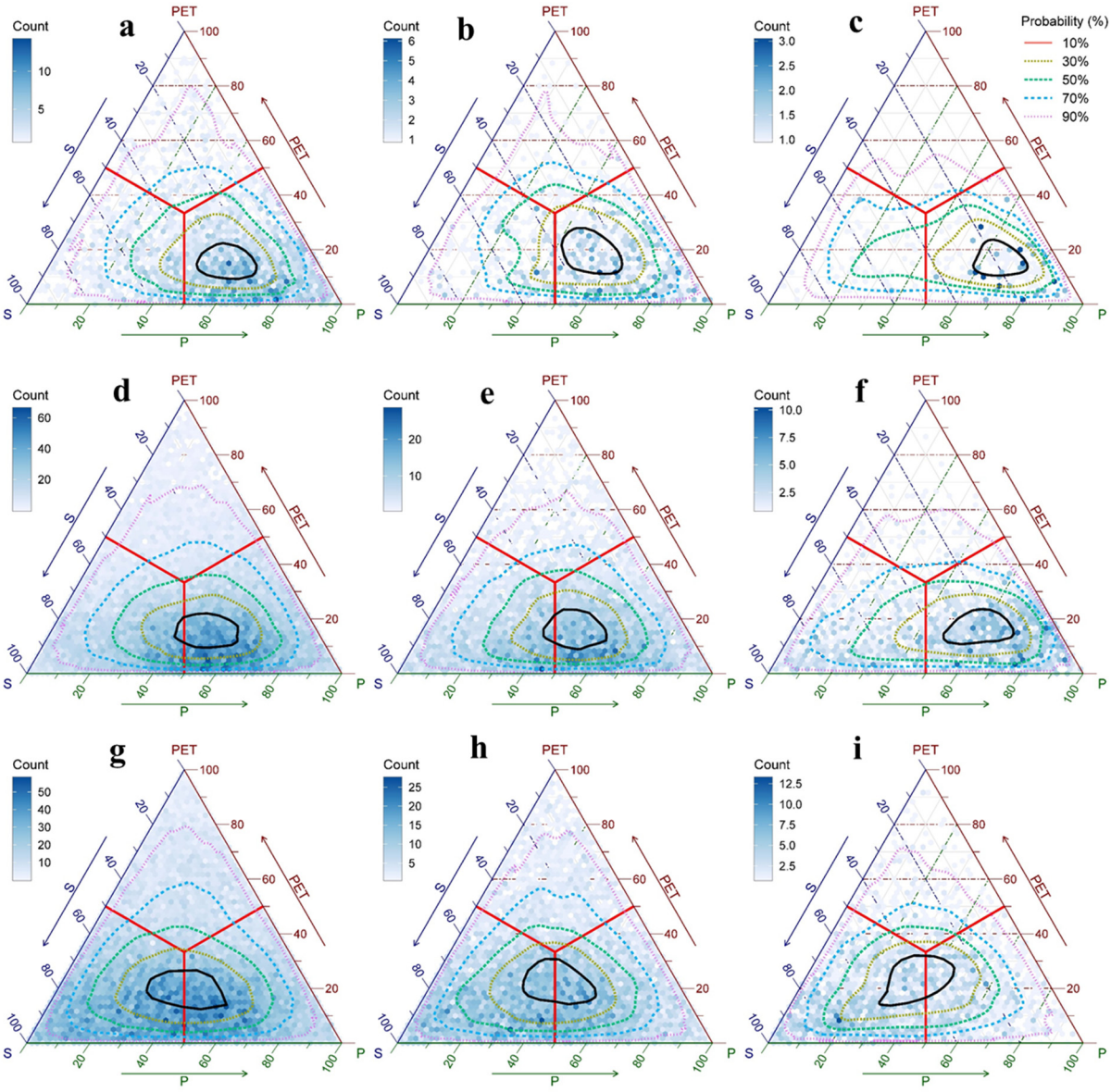

Figure S28. Same as Figure S7 for monthly (**a,d,g**), seasonal (**b,e,h**) and annual (**c**,**f,i**) scales and for different climate regimes (top three panels (**a**–**c**) for energy-limited, middle three panels (**d**–**f**) for equitant, bottom three panels (**g**–**i**) for water-limited), but the relative contributions obtained from precipitation, potential evaporation, and groundwater recharge simulated from four global hydrological models in 1351 catchments. There are total of 4 combinations obtained from the four global hydrological models.